AIAA JOURNAL
Vol. 35, No. 1, January 1997

Numerical Modeling of Buckling of Ring-Stiffened Cylinders

Srinivasan Sridharan* and Jessica Alberts†
Washington University, St. Louis, Missouri 63130-4899

The questions regarding the most effective technique of modeling stiffened shells persist despite the extensive literature available. In this study, ring-stiffened cylinders having widely varying radius-to-thickness ratios are analyzed by using alternative approaches for determination of their buckling strength under pressure. The approaches considered here are 1) linear stability analysis using a two-dimensional model, 2) linear stability analysis using a three-dimensional model, 3) nonlinear bifurcation analysis using a two-dimensional model, and 4) nonlinear bifurcation analysis using a three-dimensional model. In-house computer programs based on *p*-version ring elements have been developed for these approaches. A homogenization technique has been utilized for treating composite laminates made of a large number of repetitions of a basic sequence of plies. The results are compared with those given by currently available computer codes such as BOSOR, ABAQUS, and others. For thin shells, linear stability analysis can significantly overestimate the buckling capacity. For moderately thick shells, the linear and nonlinear approaches give close results for overall buckling but can differ significantly for local buckling. This is largely due to end effects where the buckling mode is localized. For two-dimensional models, the precise manner of connecting the shell and stiffener seems to be important. As may be expected, as the thickness of the shell or the stiffener increases, the two-dimensional models are found to be less and less accurate.

Introduction

STIFFENED cylindrical shells serve as structural components in a number of naval and aerospace structural systems. Buckling is the principal cause of failure of such shells. Shells fabricated from high-strength materials such as fiber-reinforced plastics fail by buckling that is initiated in the elastic range. There are several questions about the most effective technique of modeling the buckling phenomena in such stiffened shells. This paper explores some of these issues.

The literature on buckling of stiffened cylinders is vast and formidable and will not be reviewed here. The developments up to the 1970s are summarized in several publications (see, for example, Ref. 1). In the late 1970s and early 1980s, Bushnell developed computer programs of increasing levels of generality (versions of BOSOR) for the buckling of shells of revolution carrying ring stiffeners. These programs are widely used in practical design and are discussed in detail by Bushnell.[2] However, the attention was focused primarily on thin metallic shells. A significant contribution to the subject of stiffened shells was made by Arbocz and his coworkers.[3,4] In particular, Arbocz has highlighted the importance of taking account of prebuckling nonlinearities for a reliable prediction of buckling pressures.[4]

In this paper, we consider the problem of cylinders carrying internal ring stiffeners subjected to hydrostatic pressure—a familiar problem of pressure hull in naval vessels. The response of such a structure is governed by two distinct modes of buckling and sometimes by their interaction.[5]

1) Local buckling. In this mode, the shell undergoes buckling between the stiffeners with several waves running in the circumferential direction. The nodes of the waves running in the longitudinal direction coincide with the stiffeners. The stiffeners act as a support that inhibits the movement of the shell in the radial direction.

2) Overall or global buckling. This is a long-wave mode of buckling in which the stiffeners are pulled in and out in the radial direction. In the circumferential direction, this mode can be characterized by a relatively small number of waves.

In the present paper, the validity of the simplifying assumptions in modeling the buckling is examined by using numerical examples of relevance in current practice. A three-dimensional nonlinear bifurcation model is taken as the datum against which two-dimensional linear, two-dimensional nonlinear, and three-dimensional linear models are compared. The two-dimensional models are based on Sander's theory modified suitably to account for first-order shear deformation effects. The measure of comparison is the buckling pressure of stiffened cylinders. Examples with a wide range of mean radius (R)-to-thickness (h) ratios (175–50) subjected to both dead pressure (radially directed) and live pressure (truly hydrostatic pressure, which is always normal to the deformed surface) are considered. The results of earlier studies are invoked to lend support to the present results. The governing modes of buckling are identified where appropriate as local or overall.

Received Jan. 1, 1996; revision received Aug. 22, 1996; accepted for publication Aug. 31, 1996; also published in *AIAA Journal on Disc*, Volume 2, Number 1.

*Professor, Department of Civil Engineering. Member AIAA.
†Graduate Student, Department of Civil Engineering.

Theory

In-house software was developed in the interests of flexibility required for the comparative studies. The titles of the programs carry a prefix of either LIN or NONLIN depending on whether the approach taken is one of linear or nonlinear bifurcation analysis. A suffix of 2D or 3D is attached to indicate whether a two-dimensional or a three-dimensional formulation is employed. Thus, we have the following programs: LIN2D, NONLIN2D, LIN3D, and NONLIN3D. This section contains the theoretical formulation employed therein.

Cylinder Geometry

The geometry, principal material axes, and global coordinate axes of a typical cylindrical shell are shown in Fig. 1. The principal material coordinate system is shown by the coordinate axes labeled 1, 2, and 3. The axes 1 and 2 are, respectively, the in-plane principal axes parallel to and perpendicular to the fibers, respectively. Axis 3 is the outward normal at any point. (Similar definitions are applicable to the stiffeners as well.) Also shown in Fig. 1 is the global coordinate system x, r, and θ standing, respectively, for the longitudinal, the radial, and the circumferential axes as well as the loads acting on the shell, namely, an axial thrust P delivered to the ends and an external pressure q_o on the curved suface. Note that x direction, which will be referred to as the global longitudinal direction, becomes the thickness direction for the stiffener. Likewise the global r direction of the shell is the thickness direction for the shell but lies in the plane of the stiffener. Ψ is the angle between the principal material axes 1 and 2 with the axes x and θ for the shell (and r and θ for the stiffener).

Figure 2a shows the coordinate axes in the longitudinal view of the shell and the reference and material coordinate axes with respect to a cross-sectional view of a ring stiffener. L, h, and R_o refer to the cylinder length, shell thickness, and the inner radius of the cylinder.

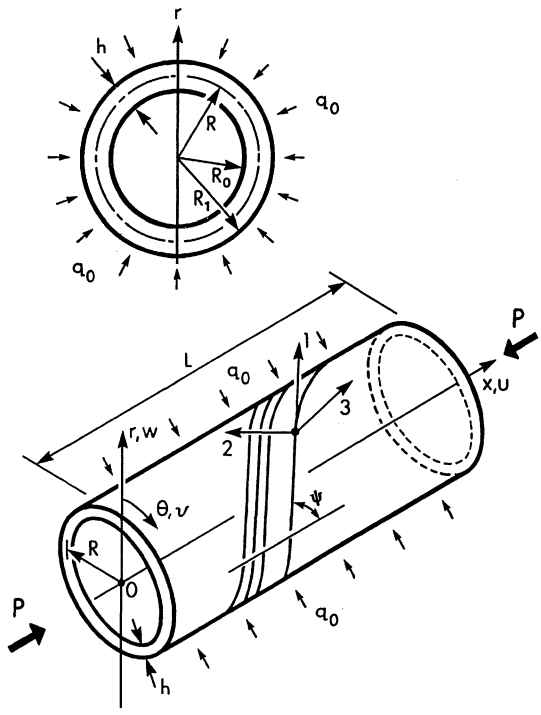

Fig. 1 Cylinder with the coordinate systems, key dimensions, and loading.

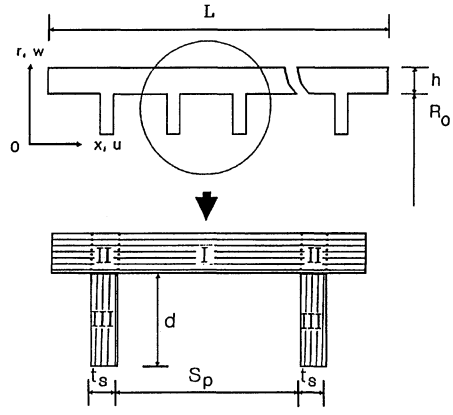

a)

b)

Fig. 2 Ring stiffened shell: a) longitudinal section and b) typical bay with three types of elements: I, shell skin; II, junction; and III, stiffener.

As shown in Fig. 2b, the clear spacing between stiffeners is S_p, the clear depth of the stiffeners is d, and the width of the stiffeners is t_s. S_p and d (not shown) are, respectively, the center-to-center distance between the stiffeners and the depth of the stiffener measured up to the center line of the shell.

Displacements

A displacement-based finite element methodology is used. Because buckling takes place in the form of a single harmonic in the circumferential direction, rotational shell elements with harmonic shape functions in the circumferential direction are employed in the analysis.

The basic variables of the three-dimensional models are the displacements u, v, and w in the x, θ, and r directions, respectively, and they vary freely in the thickness direction. In the two-dimensional formulation, on the other hand, this variation of the displacement components is accounted for by introduction of the two rotational degrees of freedom α and β. Thus, there are five variables, namely, the in-plane displacements u_o, v_o, w_o of the midsurface and α and β. Both the shell and the stiffener elements are represented by their center lines in the present treatment. With respect to the global coordinate axes, α for both the shell and stiffener elements is a rotation of the normal in the longitudinal–radial ($x-r$) plane, which must be matched at the junction. However, the β rotations for the shell and stiffener elements do not match at the junction. For the shell elements, β is a rotation of the normal in the global radial–circumferential ($r-\theta$) plane. For the stiffener elements, β is a rotation in the global longitudinal–circumferential ($x-\theta$) plane.

Constitutive Relations

Two-Dimensional Models

For the two-dimensional models, the relationship between the laminate stresses and strains can be represented in the following manner:

$$\{\sigma\} = [C]\{\epsilon\} \tag{1}$$

where $[C]$ is a matrix that describes the constitutive relations based on the elastic material constants and is computed for each element. The stresses represented by $\{\sigma\}$ are

$$\{\sigma\} = \{N_x \quad N_\theta \quad N_{x\theta} \quad M_x \quad M_\theta \quad M_{x\theta} \quad Q_x \quad Q_\theta\}^T \tag{2}$$

where N, M, and Q are, respectively, the relevant in-plane forces, out-of-plane shears, and moments per unit length. The associated strains represented by $\{\epsilon\}$ are

$$\{\epsilon\} = \left\{\epsilon_x^0 \quad \epsilon_\theta^0 \quad \gamma_{x\theta}^0 \quad \chi_x \quad \chi_\theta \quad \chi_{x\theta} \quad \gamma_{rx} \quad \gamma_{r\theta}\right\}^T \tag{3}$$

ϵ_x^0, ϵ_θ^0, and $\gamma_{x\theta}^0$ are the strains at the middle surface. χ_x is the bending curvature in the $x-r$ plane, χ_θ is the bending curvature in the $r-\theta$ plane, and $\chi_{x\theta}$ is the twist of the middle surface. γ_{rx} and $\gamma_{r\theta}$ are the transverse shearing strains. The $[C]$ matrix takes the form

$$[C] = \begin{bmatrix} [A] & [B] & 0 & 0 \\ [B] & [D] & 0 & 0 \\ 0 & 0 & e & 0 \\ 0 & 0 & 0 & f \end{bmatrix} \tag{4}$$

where $[A]$, $[B]$, and $[D]$ are each 3×3 matrices and are obtained by integration of the layer properties across the thickness[6]; e and f are given by

$$e = kG_{xr}t \tag{5a}$$

$$f = kG_{\theta r}t \tag{5b}$$

where the G are the relevant averaged transverse shear moduli. $k(=\frac{5}{6})$ is the Reissner–Mindlin shear correction factor, and t is the thickness of the laminate. Similar relationships are written for the stiffener interchanging x and r.

Three-Dimensional Models

For the three-dimensional models, the relationship between the stresses and strains with respect to the global coordinate system is represented in the general form

$$\sigma_i = C_{ij}\epsilon_j \qquad (i, j = 1, 6) \tag{6}$$

For purposes of future discussion, it is useful to view the six stress components as being made of two groups, three in-plane stress components $\{\sigma_i\}$, ($\sigma_x, \sigma_\theta, \tau_{x\theta}$ for the shell and $\sigma_r, \sigma_\theta, \tau_{r\theta}$ for the stiffener), and three out-of-plane stress components $\{\sigma_o\}$, ($\sigma_r, \tau_{r\theta}, \tau_{rx}$ for the shell and $\sigma_x, \tau_{x\theta}, \tau_{xr}$ for the stiffener). (Here σ stands for the relevant normal stress components and τ stands for the relevant shear stress components.) Likewise, it will be convenient to divide the strain components into two groups, $\{\epsilon_i\}$ and $\{\epsilon_o\}$, the in-plane and out-of-plane components.

In the treatment of the stiffeners, it was found expedient to set σ_x, the out-of-plane normal stress, equal to zero to achieve superior numerical conditioning.[5] We thus eliminate the corresponding strain and compute the effective stiffnesses $\bar{C}_{ij}$.

Homogenized Material Model

In general, there are two alternative approaches to treating a layered structure in a three-dimensional finite element analysis. The first is the discrete approach in which numerical integrations are performed layer by layer for the determination of stiffnesses. This procedure is necessary when the number of layers is small or when the lamination cannot be viewed as being made up of a sequence that repeats itself many times over. This was the approach employed in the earlier work of Kasagi and Sridharan[5] and is the basis of the INSTAAC program.[7]

The second approach is to replace the laminate by an equivalent homogeneous one.[8] This approach is applicable when the laminate is composed of a large number of repeating sequences of a small number of plies, for example a [90/0/90] or [45/−45] group repeated 100 times over. The repeating sequence of plies is henceforth referred to as the constituting ply unit. Laminates built up in this manner are apt to be thick (0.25 in. or more) and free of bending–stretching coupling and would be specially orthotropic provided the repeating unit is composed of 0/90 plies or has as many $+\theta$ plies as $-\theta$ plies.

In treating these laminates, we introduce the following two idealizations. 1) The material stiffness at any point across the thickness is equivalent to that of the basic constituting ply unit, i.e., it is the aggregate of all the individual laminae within the repeating group of plies. However, in determining this effective stiffness, continuities of in-plane strains and out-of-plane stresses have to be maintained. This leads to the second idealization. 2) The in-plane strains (ϵ_i) and out-of-plane stresses (σ_o) within a constituting ply unit are taken as constants, i.e., given by a set of values common to all the plies within the group. These idealizations are satisfied to an increasing degree as the constituting ply units increase in number.

The following are the steps to establishing the stiffness at any point in the laminate.

1) A relationship between in-plane stresses (σ_i) and out-of-plane strains (ϵ_o) on the one hand and the in-plane strains and out-of-plane stresses on the other is first established for each lamina (identified as the kth) by the partial inversion of the constitutive relationships as in the following.

Now, the stress–strain relationships are written in the partitioned form for a typical (say kth) lamina in a partially inverted form:

$$\begin{Bmatrix} \sigma_i \\ \epsilon_o \end{Bmatrix}^k = \begin{bmatrix} P_{ii} & P_{io} \\ -P_{io}^T & P_{oo} \end{bmatrix}^k \begin{Bmatrix} \epsilon_i \\ \sigma_o \end{Bmatrix}^k \tag{7}$$

2) Next, we introduce the notion of averaged in-plane stresses $\bar{\sigma}_i$ and averaged out-of-plane strains $\bar{\epsilon}_o$ for the group of plies, given by

$$\begin{Bmatrix} \bar{\sigma}_i \\ \bar{\epsilon}_o \end{Bmatrix} = \sum_{k=1}^{N} \left(\frac{t^k}{t} \right) \begin{Bmatrix} \sigma_i \\ \epsilon_o \end{Bmatrix}^k \tag{8}$$

where t^k is the thickness of the kth ply, t is the total thickness of the unit, and N is the total number of laminae within the unit. $\bar{\sigma}_i$ and $\bar{\epsilon}_o$ may be viewed as the in-plane stresses and out-of-plane strains for the point in question in the homogenized laminate.

Now, insisting that ϵ_i and σ_o are constant for all the plies in the unit, we may simply write

$$\begin{Bmatrix} \epsilon_i \\ \sigma_o \end{Bmatrix}^k = \begin{Bmatrix} \epsilon_i \\ \sigma_o \end{Bmatrix} \tag{9}$$

Using Eq. (9) in Eq. (7), the summation in Eq. (8) leads to

$$\begin{Bmatrix} \bar{\sigma}_i \\ \bar{\epsilon}_o \end{Bmatrix} = \begin{bmatrix} \bar{P}_{ii} & \bar{P}_{io} \\ -\bar{P}_{io}^T & \bar{P}_{oo} \end{bmatrix} \begin{Bmatrix} \epsilon_i \\ \sigma_o \end{Bmatrix} \tag{10}$$

where $[\bar{P}]$ is the weighted sum of the $[P]^k$ matrix of Eq. (8) as follows:

$$[\bar{P}] = \sum_{k=1}^{N} \left(\frac{t^k}{t} \right) [P]^k \tag{11}$$

3) Equation (10) is now partially inverted to yield the constitutive relationships in the form of Eq. (6).

Strain–Displacement Relationships

Three-Dimensional Model

Standard three-dimensional relationships in polar coordinates are invoked. For the shell, only the out-of-plane displacement w is considered large, whereas for the stiffener both the out-of-plane displacement u and the radial displacement w are considered large. The actual strain–displacement relationships are given in earlier publications[5,9] and will not be recounted here.

Two-Dimensional Model

This is based on Sander's theory[10] in which the first-order shear deformations are incorporated. Thus, we have

$$\epsilon_x^0 = \frac{\partial u_o}{\partial x} + \frac{1}{2}\left(\frac{\partial w_o}{\partial x} \right)^2 \tag{12a}$$

$$\epsilon_\theta^0 = \frac{1}{R}\frac{\partial v_o}{\partial \theta} + \frac{w_o}{R} + \frac{1}{2R^2}\left(\frac{\partial w_o}{\partial \theta} - v_o \right)^2 \tag{12b}$$

$$\gamma_{\theta x}^0 = \frac{\partial v_o}{\partial x} + \frac{1}{R}\frac{\partial u_o}{\partial \theta} + \frac{1}{R}\left(\frac{\partial w_o}{\partial \theta} - v_o \right)\left(\frac{\partial w_o}{\partial x} \right) \tag{12c}$$

$$\chi_x = \frac{\partial \alpha}{\partial x} \tag{12d}$$

$$\chi_\theta = \frac{\partial \beta}{R\partial \theta} \tag{12e}$$

$$\chi_{x\theta} = \frac{\partial \alpha}{R\partial \theta} + \frac{\partial \beta}{\partial x} \tag{12f}$$

$$\gamma_{rx} = \alpha + \frac{\partial w_o}{\partial x} \tag{12g}$$

$$\gamma_{r\theta} = \frac{1}{R}\frac{\partial w_o}{\partial \theta} + \beta - \frac{v_o}{R} \tag{12h}$$

Likewise, for the stiffener

$$\epsilon_r^0 = \frac{\partial w_o}{\partial r} + \frac{1}{2}\left[\left(\frac{\partial u_o}{\partial r} \right)^2 + \left(\frac{\partial w_o}{\partial r} \right)^2 \right] \tag{13a}$$

$$\epsilon_\theta^0 = \frac{1}{r}\frac{\partial v_o}{\partial \theta} + \frac{w_o}{r} + \frac{1}{2r^2}\left[\left(\frac{\partial u_o}{\partial \theta} \right)^2 + \left(\frac{\partial w_o}{\partial \theta} \right)^2 \right] \tag{13b}$$

$$\gamma_{r\theta}^0 = \frac{1}{r}\frac{\partial w_o}{\partial \theta} + \frac{\partial v_o}{\partial r} - \frac{v_o}{r} + \frac{1}{r}\left[\left(\frac{\partial u_o}{\partial \theta} \right)\left(\frac{\partial u_o}{\partial \theta} \right) + \left(\frac{\partial w_o}{\partial r} \right)\left(\frac{\partial w_o}{\partial \theta} \right) \right] \tag{13c}$$

$$\chi_r = \frac{\partial \alpha}{\partial r} \tag{13d}$$

$$\chi_\theta = \frac{\partial \beta}{r\partial \theta} \tag{13e}$$

$$\chi_{r\theta} = \frac{\partial \alpha}{r\partial \theta} + \frac{\partial \beta}{\partial r} \tag{13f}$$

$$\gamma_{\theta x} = \beta + \frac{1}{r}\frac{\partial u_o}{\partial \theta} \tag{13g}$$

$$\gamma_{rx} = \alpha + \frac{\partial u_o}{\partial r} \tag{13h}$$

Note that for the stiffener, nonlinear terms in w_o (in-plane, radial displacement) are included in Eqs. (13a–13c) to account for the significant radial movement of the stiffeners during overall buckling.

To facilitate further discussion, we introduce the L operators first introduced by Budiansky.[11] Note that any strain ϵ_i can in general

be expressed as a sum of terms that are, respectively, linear and quadratic in displacement. Thus,

$$\epsilon_i = L_{1_i}(\boldsymbol{u}) + \tfrac{1}{2}L_{2_i}(\boldsymbol{u}) \tag{14}$$

where L_1 is a linear operator and L_2 is a quadratic operator. When the displacement is made up of two contributions, i.e., $\boldsymbol{u} = \boldsymbol{u}^A + \boldsymbol{u}^B$, it is useful to define a bilinear operator L_{11} in the following manner:

$$L_{2_i}(\boldsymbol{u}^A + \boldsymbol{u}^B) = L_{2_i}(\boldsymbol{u}^A) + 2L_{11_i}(\boldsymbol{u}^A, \boldsymbol{u}^B) + L_{2_i}(\boldsymbol{u}^B) \tag{15}$$

Thus, the total strain can be expressed in terms of $\boldsymbol{u}^A$ and $\boldsymbol{u}^B$ as follows:

$$\epsilon_i = L_{1_i}(\boldsymbol{u}^B) + \tfrac{1}{2}L_{2_i}(\boldsymbol{u}^B) + L_{1_i}(\boldsymbol{u}^A) + \tfrac{1}{2}L_{2_i}(\boldsymbol{u}^A) + L_{11_i}(\boldsymbol{u}^A, \boldsymbol{u}^B) \tag{16}$$

Bifurcation Analysis

The difference between the linear and nonlinear bifurcation analyses is that in the former the critical pressure is a function of the prebuckling stress $\boldsymbol{\sigma}^{(0)}$ only, whereas for the latter it is a function of both the prebuckling stress and axisymmetric prebuckling displacements $\boldsymbol{u}^{(0)}$. It will be presumed that both $\boldsymbol{u}^{(0)}$ and $\boldsymbol{\sigma}^{(0)}$ are available for given external pressure q_o. The axial load P plays a role only in the prebuckling analysis and does not explicitly enter the bifurcation analysis, whereas the lateral pressure, if it is live, plays a role in the bifurcation analysis as well.

Even though the subject of nonlinear bifurcation is well understood,[12] the methodology adopted in the present work will be briefly presented with a view to highlight its special features and document the same in a notation that the authors believe to be succinct. The formulation for the classical linear bifurcation is obtained by simply dropping certain terms that give the influence of prebuckling displacements in the solution of the buckling problem.

It will be assumed that a solution to the nonlinear prebuckling (unbuckled axisymmetric) state is found by using a standard incremental technique, and, at the end of a given load step, the current state of stress, strain, and displacement ($\boldsymbol{\sigma}^{(0)}$, $\boldsymbol{\epsilon}^{(0)}$, and $\boldsymbol{u}^{(0)}$) is available. An approximation to the bifurcation point is obtained by extrapolating the unbuckled equilibrium path along the current tangent to the equilibrium path and looking for bifurcation on this tangent. This is done by setting up and solving for a linear eigenvalue problem for determination of the difference ($\bar{\lambda}$), respectively, between the projected bifurcation load (λ_A) and the current load carried by the structure (λ_o). This calculation is performed at the end of every step and as the solution advances, $\bar{\lambda} \to 0$, while λ_A approaches the correct bifurcation load.

Formulation for the Buckling Analysis

Let A be a point ($\boldsymbol{\sigma}^A$, $\boldsymbol{\epsilon}^A$, $\boldsymbol{u}^A$) on the unbuckled path at which bifurcation takes place and B be a point on the buckled path arbitrarily close to A. Let the change in the state from A to B be given by ($\boldsymbol{\sigma}^B$, $\boldsymbol{\epsilon}^B$, $\boldsymbol{u}^B$). The potential energy associated with the buckling process can be shown to be given by[14]

$$\Pi = \tfrac{1}{2}\sigma^B_{i,L}\epsilon^B_{i,L} + \sigma^A_i\epsilon^B_{i,NL} \tag{17}$$

where the subscripts L and NL stand, respectively, for that part of the stress or strain that is linearly and nonlinearly dependent on $\boldsymbol{u}^B$. In this expression, there are two quantities that are dependent on prebuckling quantities at the point of bifurcation A, as yet unknown. The first is obviously the state of stress given by σ^A_i. The other is $\epsilon^B_{i,L}$, which in a nonlinear context depends on $\boldsymbol{u}^A$ as

$$\epsilon^B_{i,L} = L_{1_i}(\boldsymbol{u}^B) + L_{11_i}(\boldsymbol{u}^A, \boldsymbol{u}^B) \tag{18a}$$

and the nonlinear part of the strain associated with buckling may be written as

$$\epsilon^B_{i,NL} = \tfrac{1}{2}L_{2_i}(\boldsymbol{u}^B) \tag{18b}$$

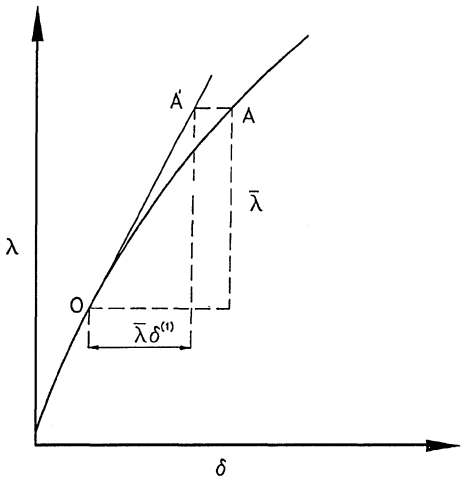

Fig. 3 Approximation of nonlinear bifurcation point A on the unbuckled path.

Nonlinear Bifurcation

Because the quantities defining the state A (Fig. 3) that occur in Eq. (17) are unknown, we approximate them in terms of the known values at O as

$$\sigma^A_i = \sigma^{(0)}_i + \bar{\lambda}\sigma^{(1)}_i; \qquad \epsilon^A_i = \epsilon^{(0)}_i + \bar{\lambda}\epsilon^{(1)}_i; \qquad u^A_i = u^{(0)}_i + \bar{\lambda}u^{(1)}_i \tag{19}$$

where $\bar{\lambda}$ is unknown. $\sigma^{(1)}_i$, $\epsilon^{(1)}_i$, and $u^{(1)}_i$ are, respectively, the stresses, strains, and displacements associated with an assumed linear response of the structure for unit increment in the load parameter. The assumption of linear response would be valid if $\bar{\lambda}$ is sufficiently small. By virtue of Eqs. (18a) and (19), $\epsilon^B_{i,L}$ and $\sigma^B_{i,L}$ can be expressed in the following forms:

$$\epsilon^B_{i,L} = L_{1_i}(u^B) + L_{11_i}(u^B, u^0) + \bar{\lambda}L_{11_i}(u^B, u^{(1)}) \tag{20a}$$

$$\sigma^B_{i,L} = D_{ij}\epsilon^B_{j,L} = D_{ij}\left[L_{1_j}(u^B) + L_{11_j}(u^B, u^0) + \bar{\lambda}L_{11_j}(u^B, u^{(1)})\right] \tag{20b}$$

Substituting Eqs. (20a) and (20b) into Eq. (17), expanding and rearranging the terms, and neglecting $\bar{\lambda}^2$ terms, we obtain

$$\Pi = \left[\tfrac{1}{2}D_{ij}\left(L_{1_i}L_{1_j} + 2L_{11_i}L_{1_j} + L_{11_i}L_{11_j}\right) + \sigma^0_i\tfrac{1}{2}L_{2_i}\right] + \bar{\lambda}\left[D_{ij}L_{11_i}L_{11_j} + D_{ij}L_{11_i}L_{1_j} + \sigma^{(1)}_i\tfrac{1}{2}L_{2_i}\right] \tag{21}$$

This is quadratic in buckling displacements and with appropriate discretization will lead to a linear eigenvalue problem. This problem must be solved at the beginning of each load step or at several points along the prebuckling path until $\bar{\lambda} \to 0$ to accurately pinpoint the critical load. For the classic linear stability analysis, we simply throw out terms that involve prebuckling displacements (L_{11}) terms and solve the problem at the unloaded state ($\sigma^0_i = 0$) and set $\bar{\lambda} = \lambda$, the critical load.

Finite Element Discretization

In all the formulations, the prebuckling deformation is axisymmetric, i.e., independent of θ, and each buckling displacement varies as a $\cos(n\theta)$ or a $\sin(n\theta)$ in the circumferential direction. In particular for three-dimensional models, we take

$$u = \bar{u}(x, r)\cos(n\theta) \tag{22a}$$

$$v = \bar{v}(x, r)\sin(n\theta) \tag{22b}$$

$$w = \bar{w}(x, r)\cos(n\theta) \tag{22c}$$

and thus use two-dimensional mapping in the $x-r$ plane for the finite elements. Note, however, this formulation is restricted to specially orthotropic materials and a more general formulation would involve both sin and cos terms for each displacement. n is the number of

circumferential waves in the buckling mode. (Later n and m are employed to indicate the number of waves associated with overall and local buckling, respectively.)

The p-version finite element discretization is employed throughout. Thus, instead of increasing the number of elements in a model, the degree of the polynomial of the shape functions is increased to achieve numerical convergence of the key results. Thus, the cylindrical shell portion, the stiffener, and the junction are each represented by a single element in a bay. Complete compatibility was ensured at the interfaces of the elements.

In the case of the two-dimensional models, finite element discretization is introduced only in one direction: the global x direction for the shell and the global r direction for the stiffener. Thus, we take for the specially orthotropic material

$$\{u, w, \alpha\} = \{\bar{u}(\eta), \bar{w}(\eta), \bar{\alpha}(\eta)\}\cos(n\theta) \tag{23a}$$

$$\{v, \beta\} = \{\bar{v}(\eta), \bar{\beta}(\eta)\}\sin(n\theta) \tag{23b}$$

where η stands for either the x or the r coordinate for the shell and stiffener, respectively. The models use center-line dimensions and contain only two types of elements. The first element type is the cylinder element, which covers the center-to-center distance between successive stiffeners. The second type of element is the stiffener (ring) element, and each stiffener is represented as a single element. The shape functions used are hierarchic in nature and are based on Legendre polynomials. These have been used by the principal author and his co-workers in a number of previous publications and will not be repeated here.[5,7,9]

Hydrostatic Loading

The in-house software has two different options for modeling hydrostatic pressure: 1) dead or radial loading is a centrally directed pressure condition and 2) live or fluid loading is a pressure loading that remains normal to the surface of the deformed cylinder. The discrepancy between the two types of loading decreases as the number of waves in the circumferential direction becomes large compared to unity, as in the phenomenon of local buckling.

The fluid pressure loading case is still conservative, and a potential function can be written. The derivation can be achieved by considering the change in the volume enclosed by the cylinder as deformation occurs. The cylinder thickness does not change much during deformation, so its effect can be neglected. In general, the expression for the loss of potential due to fluid pressure loading consists of both linear and quadratic terms. In setting up the potential energy equation for the buckled state, the linear terms vanish and only quadratic terms remain. The additional quadratic terms in the potential energy function due to live fluid pressure[13] are given by

$$V_f = \frac{1}{2}q_0 \iint \left[w\left(\frac{\partial u}{\partial x}\right) - \left(\frac{\partial w}{\partial x}\right)u + \frac{1}{R_1}\left[v^2 - v\left(\frac{\partial w}{\partial \theta}\right) + \left(\frac{\partial w}{\partial \theta}\right)w + w^2 \right] \right] R_1 dx\, d\theta \tag{24}$$

where the integration is carried out over the surface of the cylinder. The fluid pressure loading formulation in the in-house programs LIN2D, NONLIN2D, LIN3D, and NONLIN3D includes all of the terms in Eq. (24), whereas INSTACC's formulation omits the first two terms involving u and w.

Numerical Studies

The in-house programs have been extensively checked for accuracy and convergence. The relevant details have been presented elsewhere.[14] The focus of this study is essentially on the following two aspects of analytical modeling of cylinders: 1) linear prebuckling formulation vs nonlinear prebuckling formulation and 2) two-dimensional analysis vs three-dimensional analysis. The results of a buckling analysis will be influenced by other aspects of modeling too, such as live (fluid) pressure loading vs dead radial loading and use of the homogenization technique in three-dimensional analysis. These aspects will also be briefly touched upon.

Benchmark Problems

Ring-stiffened cylinders having the following description are studied and the results obtained are compared to results obtained by using generally accepted computer codes whenever available.

1) An isotropic, thin ($R/t = 173.4$) cylinder carrying six ($N_S = 6$) stiffeners. These were investigated by Moradi and Parsons[15] using a variety of commercial codes.

2) Moderately thick isotropic cylinder ($R/t = 50$) carrying 12 ($N_S = 12$) stiffeners, investigated by Arbocz using BOSOR and EPAC.[16] These cylinders were analyzed with alternative depths of rings.

3) The last cylinder studied is a layered composite ring-stiffened cylinder composed of a large number of [90/0] units, with $R/t = 100$ and 10 stiffeners ($N_S = 10$). When composed of a single unit of plies, this was analyzed by Kasagi and Sridharan[5] using INSTAAC and investigated for interactive buckling.

The key dimensions of the three-dimensional and two-dimensional models are shown in Figs. 4a and 4b, respectively. In all the calculations, symmetry with respect to center line ($x = L/2$) was exploited and only half the cylinder was modeled. The simply supported boundary conditions applied to the cylinder for each

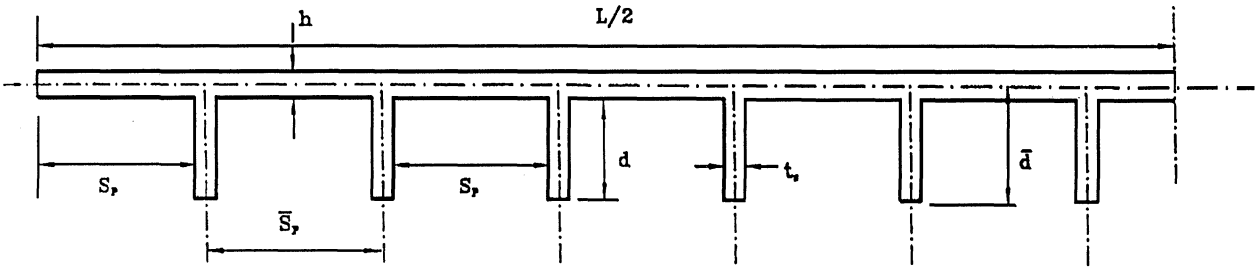

a) Three dimensional

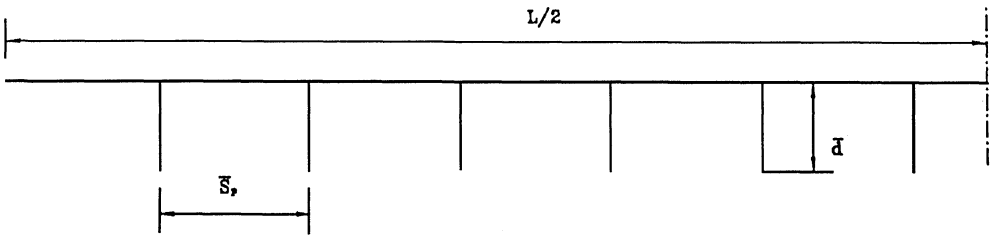

b) Two dimensional

Fig. 4 Generic model.

analysis: at $x = 0, L$, $v_o = w_o = \beta = 0$ (two-dimensional analysis); $v = w = 0$ (three-dimensional analysis). By virtue of symmetry at $x = L/2$, $u_o = \alpha = 0$ (two-dimensional analysis) and $u = 0$ (three-dimensional analysis).

The p levels (degrees of the polynomials) in the x and r directions (p_x and p_r, respectively) are chosen to contain errors within 0.5% in all cases. Typically for the shell element (element I), we use $p_x = 4$, $p_r = 2$; for stiffener, $p_r = 4$ and $p_x = 2$; and for the junction $p_r = 2$ and $p_x = 2$, thus ensuring complete compatibility at the interfaces.

Stiffened, Thin, Isotropic Cylinder (Moradi–Parsons)

The first cylinder studied is an isotropic cylinder with six ring stiffeners. A thorough study of this shell was completed by Moradi and Parsons,[15] and this study provides a benchmark for comparing current results.

The geometric data are as follows: $L = 2.38$ in. (60.452 mm); $R = 3.9885$ in. (101.31 mm); [$R_1 = 4$ in. (101.6 mm)] h = 0.023 in. (0.5842 mm); $N_s = 6$; $t_s = 0.017$ in. (0.4318 mm); and $S_p = 0.34$ in. (8.636 mm). The ratio of volume of stiffener material to that of cylinder is 0.24 based on center line dimensions, so that the stiffener depth (measured from the center line of the shell) $\bar{d} = 0.1288$ in. (3.2715 mm). The geometry of the three-dimensional models (LIN3D, NONLIN3D, INSTAACC) is derived from the center-line dimensions given above. (All bays of the two-dimensional model are of equal length, whereas the end bays of the three-dimensional models differ from the interior ones by $t_s/2$.)

The material properties are as follows: $E = 10,400$ ksi (71,705.5 MPa); $v = 0.3$. The cylinder was subjected to hydrostatic pressure in the form of radial loading.

The buckling loads obtained by Moradi and Parsons[15] using different types of elements and formulations are presented in Table 1 along with the current results. The results shown are buckling pressures for the overall mode of buckling, with seven waves in the circumferential direction.

Table 1 demonstrates the following results. 1) The close agreement of the current results shown in the bottom half of the table with the previous results shown in the top half of the table, which were obtained by standard software such as ABAQUS and BOSOR4. 2) The importance of a nonlinear prebuckling analysis. The table shows a fairly large discrepancy between the loads obtained by the linear prebuckling analysis and those obtained by the nonlinear prebuckling analysis. 3) Both two-dimensional and three-dimensional analyses give essentially the same results for the shell.

In general, for thin cylinders the buckling pressure produced by the nonlinear bifurcation analysis is significantly less than that produced by the linear bifurcation analysis. This appears to have been caused essentially by the prebuckling deformation, which alters the longitudinal profile of the shell at the ends of the cylinder. This effect is duly accounted for by the nonlinear bifurcation analysis.

Note that the overall buckling mode as generated by the linear prebuckling analysis differs greatly from that generated by the nonlinear prebuckling analysis. This is shown in Fig. 5a, which shows the overall buckling modes generated by LIN2D and NONLIN2D. For the nonlinear bifurcation analysis, the maximum radial displacement occurs near the edge of the cylinder, and for the linear bifurcation analysis the maximum radial displacement occurs at the center of the cylinder.

Table 1 Comparative study on Moradi–Parson[15] cylinder

	Buckling pressure, psi (MPa)	
Analysis program	Linear bifurcation	Nonlinear bifurcation
ABAQUS (S4R5)	298 (2.055)	261 (1.800)
ABAQUS (STR15)	309 (2.131)	——
ABAQUS (S8R5)	303 (2.089)	265 (1.827)
ABAQUS (C3D20)	307 (2.117)	274 (1.889)
BOSOR4	302 (2.082)	265 (1.827)
INSTACC	302 (2.082)	——
LIN2D	301 (2.075)	——
NONLIN2D	——	265 (1.827)
LIN3D	302 (2.082)	——
NONLIN3D	——	262 (1.806)

Only the overall buckling pressures are shown in Table 1, as this cylinder was studied for purposes of comparison, and there were no previously obtained data on local buckling pressures. As a matter of interest, the local buckling pressure determined by LIN2D was 578 psi for 17 waves in the circumferential direction. The local buckling modes as determined by LIN2D and NONLIN2D are shown in Fig. 5b. Once again, it is demonstrated that the buckling mode generated by the linear bifurcation analysis differs greatly from that of the nonlinear bifurcation analysis. The maximum modal radial displacement generated by the linear bifurcation analysis is near the center, and the maximum modal radial displacement generated by the nonlinear bifurcation analysis is near the edge of the cylinder.

To further demonstrate the importance of a nonlinear prebuckling analysis, a pressure-displacement plot for the cylinder as produced by such an analysis is shown in Fig. 5c. The representative displacement of the radial displacement plotted is the displacement 0.34 in. from the left end, which is at the location of the first stiffener. The figure clearly shows the nonlinearity of the prebuckling path prior to the bifurcation pressure of 265 psi. Note that the application of live pressure against dead loading does not change the results by more than a fraction of 1%. This is due to the relatively large number of waves associated with buckling ($m = 7$).

Stiffened, Moderately Thick, Isotropic (Arbocz) Cylinders

These two cylinders, designated as case 1 and case 2 Arbocz cylinders, are moderately thick, isotropic cylinders with 12 stiffeners. Both the Arbocz cylinders have the same geometry, with the only difference being that the case 1 cylinder has a greater depth of the stiffener than case 2. The dimensions of both cases are listed in Table 2. All the bays are of equal length in the three-dimensional model. Poisson's ratio is taken as 0.3. The cylinders were subjected to both live and dead pressures.

Tables 3 and 4 show, respectively, the overall and local buckling pressure predictions for the two cases. The pressures are rendered dimensionless by division by E. n indicates the number of waves in the circumferential direction for overall buckling, which takes the

Table 2 Dimensions of the Arbocz[3] cylinders

Dimension	Case 1	Case 2
t_s/h	1.0	1.0
R/h	50.0	50.0
S_p/h	20.0	20.0
d/h	7.6	3.0
$\bar{S}_p/h$	21.0	21.0
$\bar{d}/h$	8.1	3.5

Table 3 Overall buckling pressure predictions for Arbocz[3] cylinders

Analysis program	Dead pressure[a]	Live pressure[a]
	Case 1[b]	
EPAC	2.784	2.208
BOSOR5	——	2.254
NONLIN2D	2.301	1.913
NONLIN3D	2.286	1.939
INSTACC	2.158	1.796
LIN2D	2.157	1.827
LIN3D	2.156	1.861
	Case 2[c]	
EPAC	5.527	4.929
BOSOR5	——	4.981
NONLIN2D	5.207	4.724
NONLIN3D	5.201	4.809
INSTACC	5.208	4.775
LIN2D	5.070	4.600
LIN3D	5.206	4.814

[a]For case 1, pressure $= (q_{cr}/E) \times 10^4$; for case 2, pressure $= (q_{cr}/E) \times 10^5$.
[b]$n = 2$ for all results.
[c]$n = 3$ for all results.

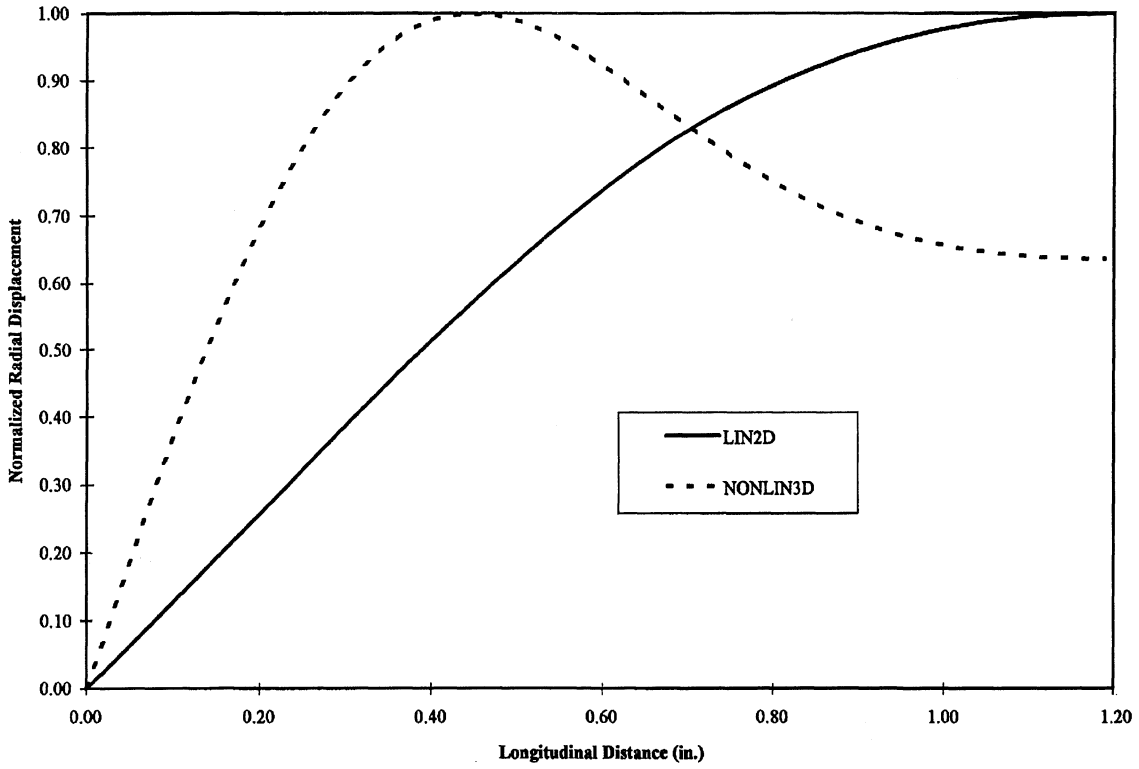

Fig. 5a Overall buckling modes of the Moradi–Parsons cylinder.

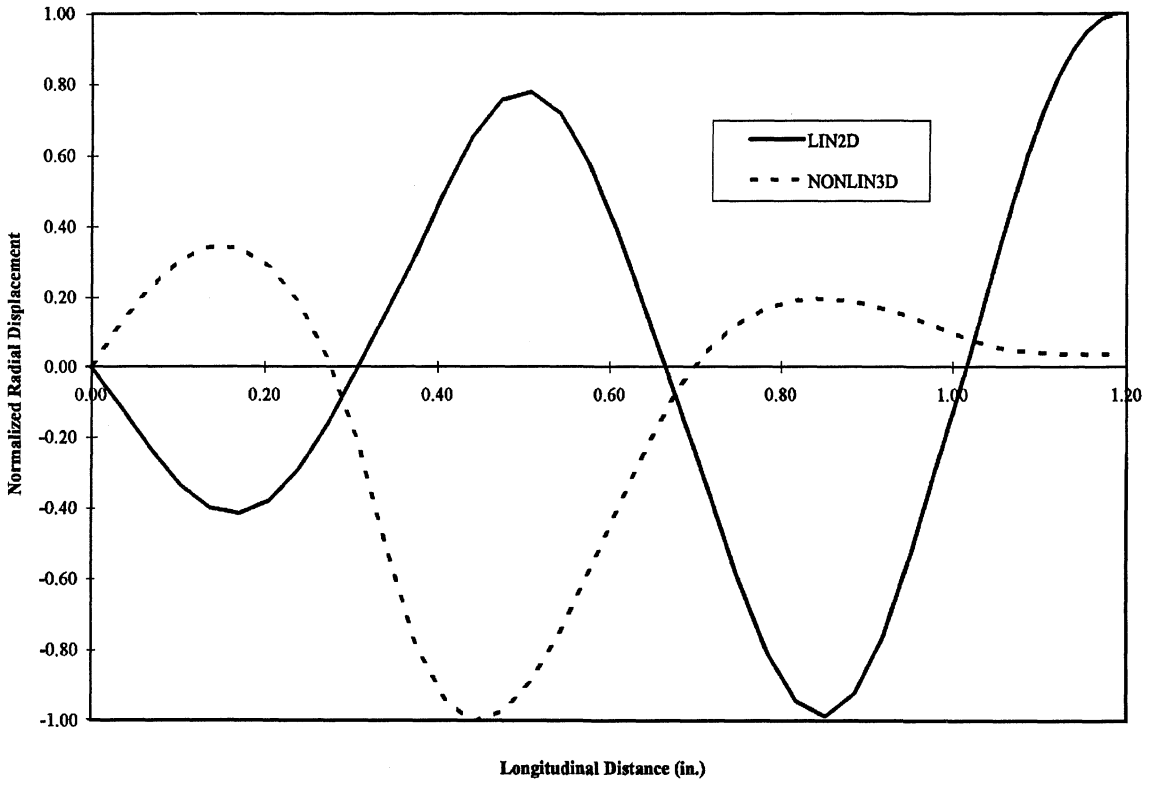

Fig. 5b Local buckling modes of the Moradi–Parsons cylinder.

values of 2 and 3, respectively, for cases 1 buckling and 2. EPAC is an elastoplastic analysis program developed by Arbocz and his coworkers.[3] BOSOR5 is developed by Bushnell.[2] Note that both EPAC and BOSOR5 perform nonlinear bifurcation analysis, so their results really can be compared only to NONLIN2D and NONLIN3D. The results reported here for BOSOR5 by Arbocz are for the fluid loading case only.

Overall Buckling Results

The most significant observation from Table 3 is that both EPAC and BOSOR5 overestimate the buckling pressures in comparison to the benchmark result of NONLIN3D, which makes no assumptions other than a linear elastic material response. The error (which is about 15% or more) is the combined result of approximations in the formulation and the manner in which stiffener is modeled.

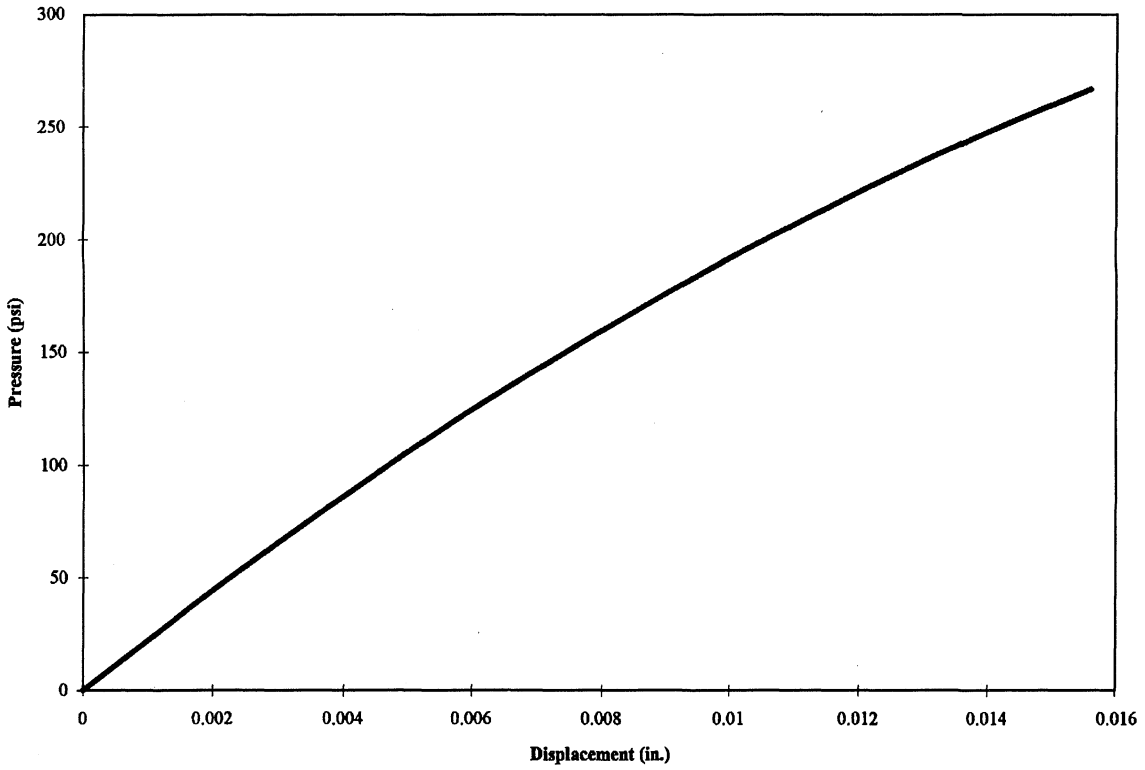

Fig. 5c Pressure vs displacement plot for the unbuckled path.

Table 4 Local buckling pressure predictions for Arbocz cylinders

Analysis program	Dead pressure, $(q_{cr}/E) \times 10^4$	Live pressure, $(q_{cr}/E) \times 10^4$
	Case 1[a]	
EPAC	1.545	1.534
BOSOR5	——	1.546
NONLIN2D	1.496	1.492
NONLIN3D	1.553	1.582
INSTACC	1.866	1.880
LIN2D	1.776	1.769
LIN3D	1.867	1.910
	Case 2[b]	
EPAC	1.543	1.501
BOSOR5	——	1.476 ($m = 8$)
NONLIN2D	1.450	1.445
NONLIN3D	1.495	1.523
INSTACC	1.758	1.772
LIN2D	1.684	1.677
LIN3D	1.759	1.798

[a] $m = 9$ for all results. [b] $m = 9$ unless otherwise indicated.

The BOSOR program 1) models the shell and stiffeners by thin shell approximations, 2) treats the stiffeners as connected to the inside of the shell, and 3) assumes that the junction region (marked as III in Fig. 2b) behaves as a thin shell. In contrast, the present two-dimensional treatment accounts for the first-order shear deformation effects and assumes the shell and stiffener are connected at the center of the shell. With respect to the connection of the stiffener with the shell, neither the BOSOR nor the present treatment can be claimed to be satisfactory for thicker shells. There is, however, greater freedom for rotation of the stiffeners in the present model and this becomes important in case 1 (which has deeper stiffeners) in the context of overall buckling. Thus, at least in this case, the present two-dimensional analyses produce results that are in better agreement with those given by the three-dimensional models. The errors associated with the present two-dimensional classical linear stability analysis (LIN2D) and two-dimensional nonlinear bifurcation analysis (NONLIN2D) are about 7 and 2%, respectively.

INSTACC and LIN3D are in excellent agreement for the dead loading case, as their formulation is identical in this case. The discrepancy in their predictions for the live-loading case can be explained as due to the omission of certain terms in INSTACC's live-loading formulation, already alluded to.

Considering case 2 (Table 3), the results of EPAC and BOSOR are much closer to the benchmark (NONLIN3D) result than for case 1. In fact, all the models perform better with the linear two-dimensional (LIN2D) giving a maximum discrepancy of 4%. This is a case of a shallower stiffener and the precise way the stiffener junction is modeled is not a major factor as far as overall buckling is concerned. Once again, BOSOR and EPAC overpredict the critical pressures slightly, whereas the present formulations are either very close to or slightly lower than NONLIN3D results.

Local Buckling Results

Table 4 summarizes the critical pressures associated with local buckling for the two Arbocz cylinders. m represents the number of waves in the circumferential direction associated with local buckling and is found to be 9 in all but one result. This is the BOSOR5 result of case 2, where $m = 8$. The point of major interest in these results is the significant difference between the critical pressures given by the nonlinear bifurcation analysis on the one hand and the classical linear bifurcation analysis (which neglects the effect of deformations altogether) on the other. The buckling modes are strongly localized near the ends because of significant prebuckling deformation near the supports—a phenomenon not picked up by the linear programs LIN2D, LIN3D, and INSTACC—and this seems to affect local buckling pressures far more than overall buckling ones. BOSOR5 and EPAC results are now in better agreement with the benchmark result (of NONLIN3D) than NONLIN2D.

Stiffened Composite Cylinder

The final example is a cylinder built up of a large number of laminae whose basic unit is given by the sequence [90/0]. The geometric data may be summarized as follows: $L/h = 262$, $R/h = 100$, $N_s = 10$, $S_p/h = 22$ (all the bays are of equal length in the three-dimensional model), $t_s/h = 2$, and $d/h = 5.422$. Note that the stiffener is somewhat stockier with $t_s/h = 2$, $d/t_s = 2.711$. The

Table 5 Buckling pressure predictions for both live and dead loading for the composite cylinder

Analysis program	Dead pressure[a]	Live pressure[b]
	Overall buckling pressure ($n = 3$)	
NONLIN2D	2.2687	2.0975
NONLIN3D	2.1123	1.9786
INSTACC	2.1016	1.9470
LIN2D	2.2530	2.0626
LIN3D	2.0976	1.9676
	Local buckling pressure ($m = 10$)	
NONLIN2D	2.3011	2.3063
NONLIN3D	2.0269	2.0532
INSTACC	2.2783	2.2815
LIN2D	2.5081	2.4970
LIN3D	2.2783	2.2956

[a]For overall buckling, pressure $= (q_{cr}/E_{11}) \times 10^5$.
[b]For local buckling, pressure $= (q_{cr}/E) \times 10^4$.

material properties (of the lamina) are as follows: $E_{11} = 16,000$ ksi (110,316 MPa), $E_{22}/E_{11} = E_{33}/E_{11} = 0.0925$, $G_{12}/E_{11} = G_{13}/E_{11} = 0.0475$, $G_{23}/E_{11} = 0.031875$; $\upsilon_{12} = 0.33$, $\upsilon_{13} = 0.33$, and $\upsilon_{12} = 0.45$.

The results of the analysis as given by the five programs, namely, LIN2D, LIN3D, INSTACC, NONLIN2D, and NONLIN3D, are given in Table 5 for overall and local buckling. Of all the programs, INSTACC alone used discrete layer properties; the rest used homogenized material properties. The results given by INSTACC approach asymptotically certain values as the number of ply groups are increased. The results were found to be unaltered up to four places beyond 40 layers (20 ply units).

Overall Buckling Results

For overall buckling ($n = 3$), the two-dimensional analyses (linear and nonlinear) give noticeably higher results than NONLIN3D with errors of 8 and 5% for dead and live loading conditions, respectively. This is essentially due to the idealizations involved in the two-dimensional models, especially regarding the action of stiffener–shell junctions. This effect is more significant in this case because of the larger thickness of the stiffener. There are other factors too of relatively minor importance in this case, such as the variation of radius from inside to outside the shell, which are not accounted for in the two-dimensional model, and shear deformation effects, which are approximately accounted for in two-dimensional models. The effects of prebuckling nonlinearities are seen to be relatively minor.

Local Buckling Results

In this case (Table 5), the effects of both the two-dimensional approximations and the prebuckling nonlinearities are both seen to be important. Comparing the results of LIN2D with NONLIN3D, for example, we have an error of more than 23% associated with the former for both the live and dead loading conditions. In comparison to the linear two-dimensional model, the nonlinear two-dimensional model does perform better but still involves an error of about 12–14%. Apparently, the stockiness of the stiffener plays a more significant role here.

Both the linear and nonlinear models indicate that the buckling modes have higher amplitudes in the bays nearer to the supports, and the buckling deflection is gradually damped out as we move to the center of the shell; however, the nonlinear models give a picture of more strongly accentuated localization near the ends. Apparently, the local buckling resistance of such shells can be significantly enhanced by a slight thickening of the end bays.

Conclusions

Algorithms for two-dimensional and three-dimensional linear and nonlinear bifurcation analyses of ring-stiffened cylinders have been reviewed. A homogenization procedure for composite shells consisting of a large number of repeating group of plies was described for three-dimensional analysis. On the basis of the case studies, the following conclusions may be drawn.

1) For thin shells ($R/h > 150$) carrying ring stiffeners, linear stability analysis not only overestimates the buckling pressures but also does not capture the correct buckling mode. Even for moderately thick shells, linear bifurcation analysis is found to be unsatisfactory when the governing mode is local. The nonlinear bifurcation analysis captures the effect of prebuckling bending deformation in the vicinity of the supports and a buckling mode, which is localized near the ends. In all these cases, nonlinear bifurcation analysis must be used. For thicker shells, which tend to buckle in the overall mode, the linear stability analysis can give an acceptable estimate for practical design.

2) For moderately thick stiffened cylinders, the precise modeling of the stiffener and shell connection is important. A simple approach in which the stiffener and the shell are both represented by their center lines and assumed to be connected at the point of intersection was found to be effective and produced results within 2% of the corresponding three-dimensional result in the case of overall buckling. The formulations (e.g., BOSOR) where the stiffener is deemed to be connected to the interior surface of the shell work satisfactorily for shallow stiffeners but can be in appreciable error for deeper stiffeners ($d/t > 8$).

3) This procedure for homogenization was found to yield accurate results when the number of repetitions of the basic unit was >20.

Acknowledgments

The research described in this paper was supported by the U.S. Office of Naval Research under Grant N00014-91-J1637 of the Ship Structures and Systems, Science and Technology Division of the Solid Mechanics Program. The constant interest and encouragement of Yapa D. S. Rajapakse, the Program Monitor, is gratefully acknowledged.

References

[1]Thompson, J. M. T., and Croll, J. G. A. (eds.), "Collapse: The Buckling of Structures in Theory and Practice," *Proceedings of IUTAM Symposium* (Univ. College, London), Cambridge Univ. Press, Cambridge, England, UK, 1983, pp. 443–527.

[2]Bushnell, D., *Computerized Buckling Analysis of Shells*, Kluwer Academic, Norwell, MA, 1985.

[3]Arbocz, J., "The Effect of Initial Imperfections on Shell Stability—An Updated Review," Faculty of Aerospace Engineering, Rept. LR-695, Delft Univ. of Technology, Delft, The Netherlands, Sept. 1992.

[4]Arbocz, J., and Hol, J. M. A. M., "On the Reliability of Buckling Load Predictions," *AIAA/ASME/ASCE/AHS/ASC 35th Structures, Structural Dynamics, and Materials Conference* (Hilton Head, SC), AIAA, Washington, DC, 1994, pp. 514–521.

[5]Kasagi, A., and Sridharan, S., "Modal Interaction in Composite Cylinders Under Hydrostatic Pressure," *International Journal of Solids and Structures*, Vol. 32, No. 10, 1995, pp. 1349–1369.

[6]Jones, R. M., *Mechanics of Composite Materials*, Hemisphere, New York, 1975, pp. 154, 155.

[7]Kasagi, A., Sridharan, S., and Schokker, A., "INSTAAC User Manual," Dept. of Civil Engineering, Washington Univ., St. Louis, MO, Feb. 1994.

[8]Pecknold, D. A., and Rahman, S., "Micromechanics-Based Structural Analysis of Thick Laminated Composites," *Computers and Structures*, Vol. 51, No. 2, 1994, pp. 163–179.

[9]Schokker, A., Kasagi, A., and Sridharan, S., "Dynamic Interactive Buckling of Ring Stiffened Composite Shells," *AIAA Journal*, Vol. 33, No. 10, 1995, pp. 1954–1962.

[10]Brush, D. O., and Almroth, B. O., *Buckling of Bars, Plates and Shells*, McGraw–Hill, New York, 1975, Chap. 6.

[11]Budiansky, B., "Dynamic Buckling of Elastic Structures: Criteria and Estimates," *Dynamic Stability of Structures*, edited by G. Herrmann, Pergamon, Oxford, England, UK, 1966, pp. 83–87.

[12]Thompson, J. M. T., and Hunt, G. W., *A General Theory of Elastic Stability*, Wiley, New York, 1973, pp. 50–81.

[13]Sewell, M. J., "On the Calculation of Potential Functions Defined on Curved Boundaries," *Proceedings of the Royal Society of London, Series A*, Vol. 286, No. 1406, 1965, pp. 402–411.

[14]Alberts, J., "Comparative Studies of Techniques for Analytical Modelling of Ring Stiffened Cylinders," M.S. Thesis, Dept. of Civil Engineering, Washington Univ., St. Louis, MO, Dec. 1995.

[15]Moradi, B., and Parsons, I. O., "A Comparison of Modelling Techniques for the Buckling of Stiffened Shells," *ASCE Engineering Mechanics Specialty Conference* (Columbus, OH), American Society of Civil Engineers, New York, 1991, pp. 856–860.

[16]Arbocz, J., private communication, Delft Univ. of Technology, Delft, The Netherlands, 1992.